A Theoretical and Molecular Dynamics Study of Mixing in Microchannels with Obstacles

E. C. J. Oliver

E-mail: eric.oliver@utas.edu.au
Institute for Marine and Antarctic Studies, University of Tasmania, Hobart, Tasmania, Australia

G. W. Slater

E-mail: gslater@uottawa.ca
Department of Physics, University of Ottawa, Ottawa, Ontario, Canada

Abstract. A system consisting of two miscible fluids in a microchannel under laminar flow has been examined with theoretical techniques and simulated using Molecular Dynamics (MD). We have applied the theory of diffusion to predict the displacement of particles as they diffuse across a channel perpendicular to a Poiseuille flow. Using MD simulations, we have studied the presence of obstacles, including a prism-shaped arrangement of posts, in the flow path and shown that (i) they increase the level of partial mixing in the vicinity of the obstacles, and (ii) they do not shorten length of channel required to obtain complete mixing. The presence of the obstacles flatten the flow profile within a certain range of the obstacles and impart a cross-channel velocity component to the flow such that it follows a sinuous path through the channel. From our theoretical predictions and numerical simulations, we show that a flattened flow profile results in increased levels of partial mixing when compared to a system lacking obstacles. However, the presence of obstacles does not reduce the channel length required to achieve full mixing due to the restrictions of laminar flow. Furthermore, cross-channel flow induced by the obstacles has the effect of increasing contact between the fluids but the mixing increase is negligible.

PACS numbers: 47.11.Mn,47.61.Ne

1. Introduction

The essential problem with efficient mixing on small scales is that, in general, flow is laminar and thus the instabilities produced by turbulent flow that accelerate the fluid mixing on macroscopic scales (such as the act of stirring cream into coffee) are no longer present. In the absence of these mixing accelerants, diffusion is the only natural drive to mixing. Laboratories would like to develop methods to enhance the effects of diffusion or introduce other phenomena into the system in order to facilitate efficient mixing at low Reynolds numbers where viscous effects dominate over inertial ones.

This problem has been well studied recently and there have been many successful attempts which involve processes such as vortices induced by curved flow [1], electroosmosis [2], electro-hydrodynamics [3], chemically and geometrically patterned channel walls [4, 5, 6], hydrodynamic focussing (nanojets) [7], and chaos [8]. Reviews of work in this field can be found in Refs. [9, 10, 11].

Several studies have investigated how the presence of immobile obstacles in a microchannel might enhance the mixing level at the output. Wang *et al.* show that certain obstacle configurations modify the fluid flow laterally and force one species into the other in a way that may promotemixing [12, 13]. It has also been shown that diamond-shaped obstacles [14] and a collection of obstacles in V-shaped configuration [15, 16] enhance mixing in low Reynolds number flows. It has been noted in most of these studies that the presence of obstacles induces a cross-channel component to the flow which may increase mixing efficiency [12, 13, 17, 15, 16].

We will demonstrate, using Molecular Dynamics simulations, that the presence of obstacles enhances partial mixing over short distances but does not decrease the channel length required for complete mixing. Obstacles enhance partial mixing primarily by distorting the flow profile and increasing the contact area between the two fluid species. However, in laminar flows the distance required to attain complete mixing is controlled by the mean flow rate. This paper is organized in three main segments. First, we will present the fluidic system along with the relevant hydrodynamic theory outlining laminar flow, the behaviour of diffusion in channels, and the concept of mixing in channel flows. Then, we will review the simulation method and how it is applied to our system. Following that, we present the results in three sections. First, we explore the laminar hydrodynamic and diffusive properties of the system. Next, we examine the mixing properties in channels without obstacles. Finally, we will introduce obstacles into the system and show that their presence affects the mixing characteristics of the system by lengthening the mixing interface as well as deforming the flow profile. It is this last effect that will be the focus of our claim that, where complete mixing is required, simple arrangements of obstacles do not increase mixing efficiency in microchannels.

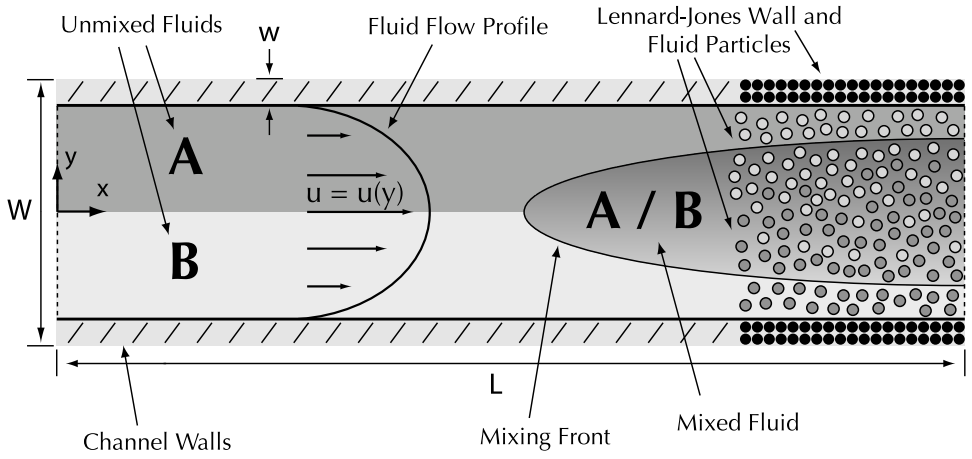

Figure 1. Schematic of the fluid-channel system. The two miscible fluid species (A and B) are separated along the midplane of the channel and travel through the channel with a Poiseuille flow profile. The fluids are allowed to mix via diffusion which produces a mixing front between the mixed and unmixed fluid. Also shown here is an example of the finite bead structure of the channel walls and fluid used in our simulations.

2. System and Theory

Consider a fluidic system such as the one shown in Fig. 1 consisting of two miscible fluid species (labelled A and B) confined between two parallel plates spaced a distance W apart. We are examining only a section of length L in the x direction. The fluid is moving in the x direction with a Poiseuille (parabolic) flow profile. The channel dimensions are on the order of micrometres and the flow is laminar.

2.1. Laminar Flow

The Reynolds number determines the basic hydrodynamic behaviour when considering fluid flow confined in channels and can be expressed as

$$\mathrm{Re} \equiv \frac{\rho_0 \bar{u} W}{\eta}, \tag{1}$$

where $\bar{u}$ is the average fluid velocity (the flow rate) over the channel cross-section of width W, η is the shear viscosity (or dynamic viscosity, sometimes denoted by μ) and ρ_0 is the average fluid density. The transition from laminar to turbulent flow can be indicated by the Reynolds number, laminar flow ocurring for $\mathrm{Re} \lesssim 10^3$ and turbulent flow for $\mathrm{Re} \gtrsim 10^3$. For hydrodynamic flow in channels whose cross section is on the order of or less than micrometers, then for reasonable $\bar{u}$ the system is firmly rooted in the realm of laminar flow. In the laminar flow regime, the flow is smooth and predictable and lacks any of the instabilities and rich eddy structure that is found in turbulent flow. The dynamics are dominated by the viscosity of the system rather than by inertial forces and the dynamics of all flows are reversible (if we neglect diffusion, which is the topic of the next section). Because of this reversibility it is not obvious how a finite forest of

obstacles can actually increase mixing. This is the topic of this investigation.

Consider a fluid confined between two plates parallel to the xz-plane with the origin of the coordinate system midway between them. For low Reynolds numbers, the flow profile generated by a pressure difference, p', along the x-direction in a channel is of the Poiseuille type and has the quadratic form

$$u(y) = u_0 \left(1 - \frac{y^2}{y_0^2}\right), \tag{2}$$

where $u_0 = -y_0^2 p'/2\eta$ and $\pm y_0$ are the positions of the two channel walls. Note that we are assuming no-slip at the boundaries, which will be sufficient for our studies (see Refs. [18, 19, 20] for explorations of slip length in Molecular Dynamics simulations of laminar flow). In practice, Poiseuille flow is usually generated by a pressure gradient along the channel but it can also be generated by a gravity-like acceleration g in which case we can make the substitution $-p' = \rho_0 g$ in Equation 2.

2.2. Diffusion

Since turbulence does not exist in a laminar flow environment, we cannot rely on it to mix the fluids as we would in a turbulent system. Therefore, the drive behind fluid mixing is the relatively slow diffusion of one fluid into the other at their interface. The Peclet number, Pe, is a measure of the relative influences of advection and diffusion for flows in channels and is defined as

$$\mathrm{Pe} \equiv \frac{\bar{u} y_0}{D}, \tag{3}$$

where D is the diffusion coefficient. We use the length scale $y_0 = W/2$ (half the cross-sectional width) since it is the largest distance in our system that particles need to diffuse in order to initiate mixing. Large Pe implies that fluid motion is dominated by advection (flow) rather than diffusion. When Pe is large, it is difficult to mix fluids by diffusion alone as a long channel (i.e., much longer than its width) is then required to allow diffusion to take its course.

The average time, $\langle t_\mathrm{D} \rangle$, needed for molecular diffusion to transport fluid a distance d in one dimension is given by the Einstein relation

$$\langle t_\mathrm{D} \rangle = \frac{d^2}{2D}. \tag{4}$$

If the fluid is being transported along the channel at a constant velocity u then we can deduce the average distance $\langle l \rangle$ the fluid travels along the channel in the flow direction while diffusing a distance d in the perpendicular direction:

$$\langle l \rangle = u \langle t_\mathrm{D} \rangle = \frac{u d^2}{2D}. \tag{5}$$

Given channel geometry and flow speed and using Equations 4 and 5 we can calculate both the time required $\langle t_\mathrm{D} \rangle$ and the total distance travelled $\langle l \rangle$ along the channel for particles diffusing a distance d from the channel centre. The choice of the initial position is important since the result shown above will be dependent on the velocity which itself

is position dependent. We choose the original position to be the centre since, as we will see later, the mixing interface originates as particles in the channel centre diffuse towards the wall). Let L_0 be the channel length where the particles have diffused the full width required: y_0. From Equations 5 and 3 this length is given by $L_0 = y_0\mathrm{Pe}/2$.

It should be noted that the above expression relating $\langle l \rangle$ and d (Equation 5) only applies for a constant velocity profile (i.e., $u(y) = u \equiv \text{const.}$). We will be examining diffusion in a channel where the flow is not flat but spatially dependent, namely a Poiseuille flow profile. The equivalent expression to Equation 5 becomes

$$\langle l \rangle = \frac{u_0 d^2}{2D}\left(1 - \frac{1}{2}\frac{d^2}{y_0^2}\right). \tag{6}$$

The first term is identical to Equation 5 and the second term involves a correction due to the quadratic nature of the flow profile. The derivation of this expression can be found in Appendix A and a graphic representation of Equations 5 and 6 can be found in Fig. 2. The phenomena presented in this figure will be discussed in the following section. We will refer to curves showing the average length along the channel a particle has travelled, $\langle l \rangle$, while diffusing a distance d (such as those deduced from Equations such as Equation 5 and Equation 6) as *flow-diffusion profiles*. Note that this entire discussion assumes that the diffusion coefficient D is independent of spatial position and identical for the two fluids. In reality, due to the presence of the rigid walls, there may be some spatial dependence [21, 22] but we will assume its effect to be negligible.

2.3. Mixing

Diffusion is inherently linked to mixing in laminar flow systems of multiple fluid species. As mentioned above, due to the lack of instabilities caused by turbulence, diffusion is the only mechanism that can mix fluids in simple laminar channel flows. As fluids of different species diffuse into each other we can qualitatively describe the level of mixing to have increased, until the point where both concentrations are equal and we would consider the fluid to be fully mixed. Later we will present a quantitative mixing function to be used with our numerical simulations, but for the following discussion consider a hypothetical measure (or disorder parameter) that is maximized when the fluids are fully mixed and zero when they are completely separated. If we examine the flow-diffusion profiles due to various flow profiles we can think of the curves as roughly corresponding to the position of the *mixing front*. By mixing front we refer to the division between unmixed fluid and mixed fluid (the region containing the latter widens as the fluids flow along the channel). In practice this front is not clearly defined since diffusion is a process which results in a wide distribution of particle positions; however this expression would correspond to the mean position of the front (or some inflection point).

Now, consider different flow profiles, $u(y)$, but with the same flow rate, $\bar{u} = \int_{-y_0}^{y_0} u(y)dy/2y_0$. Equations 5 and 6 predict that if the average flow rate is the same then a particle diffusing from the centre of the channel (where we are considering the initial interface between different fluid species to be) will travel the same length down

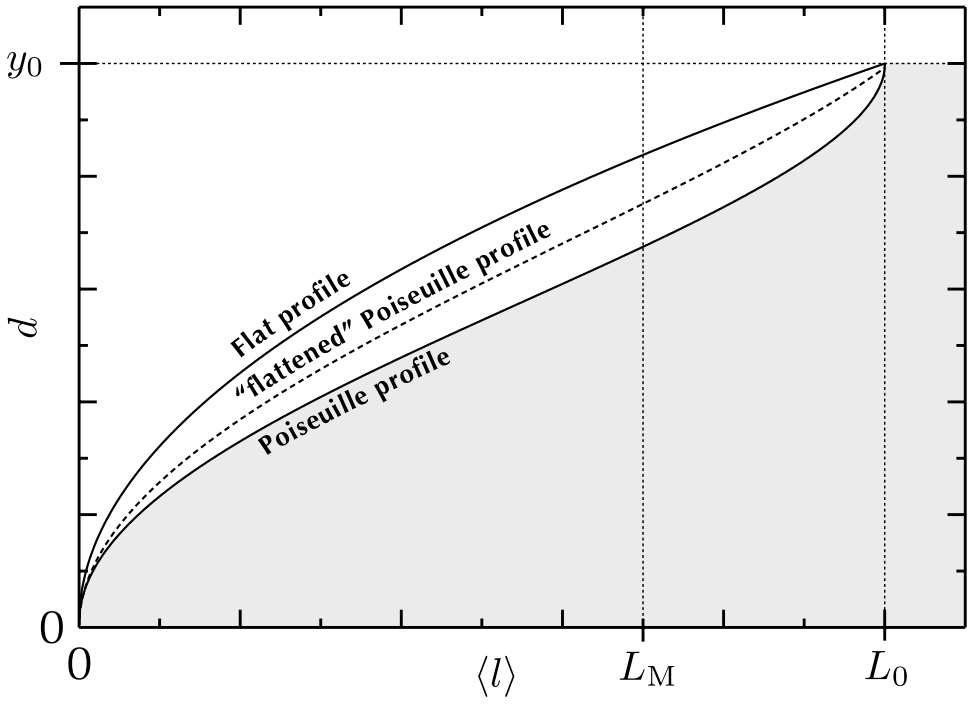

Figure 2. The flow-diffusion profile for various flows. The results are shown for both a flat profile, $u(y) = u_0/2$, and a Poiseuille profile, $u(y) = u_0(1 - y^2/y_0^2)$, as well as a general "flattened" Poiseuille flow profile lying somewhere in between. For flow profiles with the same average velocity, $\bar{u}$, particles will on average take the same channel length, L_0, to reach the channel wall, y_0, by diffusion.

the channel, $L_0 = y_0\mathrm{Pe}/2$, when it reaches the position of the wall, y_0. This is intuitive as the time taken to diffuse that distance is always the same (simply Einstein's relation $\langle t_{\mathrm{D}} \rangle = y_0^2/2D$) and so if the average velocity felt is always the same then the average distance travelled will be the same (there is no coupling between the motion in x and y). As a demonstration we have shown a hypothetical "flattened" Poiseuille flow profile (with the same average flow rate), whose d-vs-$\langle l \rangle$ curve should lie somewhere between the flat profile and the pure Poiseuille profile (as seen in Fig. 2). (A numerical method of determining this curve from the flow profile data is outlined in Appendix B.) Therefore, as long as the channel length, L, is greater than L_0 then the measured level of mixing at the channel outlet will always be 100%. However, if the channel length is less than L_0 then the measured level of partial mixing will depend on the shape of the flow profile. A flat profile will yield a higher level of mixing than a Poiseuille profile. Similarly, so will a flattened Poiseuille profile.

We will show that the primary effect produced by placing obstacles in the flow path, which is what was studied in Refs. [12, 13], is simply to flatten its quadratic flow profile so that the level of partial mixing observed at some measuring length, $L_{\mathrm{M}} < L_0$, is greater than that observed by a perfectly quadratic flow profile. However, as demonstrated above, if $L_{\mathrm{M}} \geq L_0$ then the measured level of mixing for any profile will be 100% in any case. In other words, the obstacles merely change the transient behaviour.

3. Simulation and Measurement Method

In order to substantiate our claim in Section 2.3 we will explore the mixing properties of channels with and without obstacles by explicit simulation of the fluid and solid walls. We consider the size of the system presented in Section 2 to be very large in the z direction. All forces and geometries will be isotropic in the z-direction and so we will make the approximation that the flow in any two-dimensional slice of the system parallel to the xy-plane will be identical. Therefore, we will confine our simulations to two dimensions which will both retain the essential physics as well as increase computational efficiency.

3.1. Molecular Dynamics

We model the system described in Section 2 as an ensemble of interacting beads and simulate their dynamics using the Molecular Dynamics (MD) computational algorithm. The beads obey the Lennard-Jones (LJ) potential that acts between a pair of particles i and j

$$U_{ij} = \begin{cases} 4\epsilon \left[\left(\frac{\sigma}{r_{ij}}\right)^{12} - c_{ij} \left(\frac{\sigma}{r_{ij}}\right)^{6} \right] + \epsilon_0 & \text{if } r_{ij} \leq r_c \\ 0 & \text{if } r_{ij} > r_c \end{cases} \tag{7}$$

where ϵ and σ are constants that set the energy and length scales for a particular substance. All particles in the system interact with the LJ potential except for wall-wall interactions since the positions of the wall particles are fixed (their interactions with each other are ignored). For efficient numerical operation, we do not consider the pure LJ potential up to $r = \infty$ but instead neglect long range interactions. We do this by cutting it off at a certain radius r_c so that the potential is zero for $r > r_c$ and a constant $\epsilon_0 = -U(r_c)$ is added to ensure continuity [23]. We choose $r_c = 2.5\,\sigma$ which retains the repulsive core and most of the attractive tail. The average density of the fluid is $\rho_0 = 0.8/\sigma^2$ and the thermal energy is $k_B T = 1\ \epsilon$ and all particles have mass m.

The Molecular Dynamics algorithm consists of integrating Newton's equations of motion for each particle in the system using finite difference methods. Methods such as linked neighbour and cell lists are used to facilitate the efficient operation of the algorithm [23]. It should be noted that in order to keep the temperature of the system constant a thermostat is employed and since the system we are studying is not in equilibrium we must choose a thermostat that can be applied to nonequilibrium MD. The thermostat used here is based on the method of dissipative particle dynamics (DPD) which conserves momentum and reproduces hydrodynamic interactions [24]. Care has been taken to ensure that known time step effects when using DPD are avoided [25].

As mentioned earlier, we have chosen to work in two dimensions (xy) for the simplicity of the algorithm. This can be justified as follows: if the channel size in the dimension perpendicular to the two dimensions considered (z) is much larger than its width in y then any xy slice we take should be identical. Therefore, by simulating this

slice independently we can recreate its flow characteristics. The channel we consider is rectangular in xy with walls containing the fluid along y and periodic boundary conditions along x. Three system lengths were used: $L = 55.9\,\sigma$ (for a small test system demonstrating laminar flow), $L = 447.21\,\sigma$ (for mixing in channels with obstacles) and $L = 559.02\,\sigma$ (for mixing in channels without obstacles) and the width is always $W = 55.9\,\sigma$ with the wall particles taking up a width $w = 2.24\sigma$ (two particle layers) on each side. The total number of particles in these three systems are $N = 2500$, $N = 20000$ and $N = 25000$, respectively.

3.2. Mixing Value: A Per-particle Quantification of the Mixing Level

Mixing is a highly qualitative state; qualitatively fluids can be *mixed* or *unmixed* but mixing does not have a rigid scientific definition. In the past, measures have been proposed to quantify the level of mixing between two fluids including those based on concentration in slices across the channel [12, 13] or entropy [26]. We propose an expression that will quantify the local level of mixing associated with each particle in a system of binary fluids. From there, one is free to average in many different ways in order to represent the mixing of the bulk fluid.

Our model is composed of discrete particles that have a type associated with them which defines which fluid species that particle belongs to. The method we have employed is to associate a level of mixing with each individual particle based on its surrounding environment. Consider all the particles contained within a radius r_{mix} about a given particle (particle i) ignoring the centre particle. In a binary mixture, we will have N_{L_i} particles of the same type as particle i and N_{U_i} particles of different type from particle i such that $N_i = N_{\mathrm{L}_i} + N_{\mathrm{U}_i}$ is the total number of particles contained in r_{mix}. We propose, as the expression to quantify the local level of mixing, M_i, associated with particle i, the product of N_{U_i}/N_i and N_{L_i}/N_i (both of which run from 0 to 1) and normalized to equal 1 at $N_{\mathrm{U}_i} = N_{\mathrm{L}_i} = N_i/2$:

$$M_i = 4\frac{N_{\mathrm{U}_i} N_{\mathrm{L}_i}}{N_i^2}, \tag{8}$$

So, $M = 1$ when the fluids are perfectly mixed and $M = 0$ when they are completely unmixed. This produces a function that is quadratic in N_{U_i} (or N_{L_i} since they sum to the constant N_i) with zeros at $N_{\mathrm{U}_i} = 0$ ($N_{\mathrm{L}_i} = N_i$) and $N_{\mathrm{U}_i} = N_i$ ($N_{\mathrm{L}_i} = 0$) and a value of 1 at $N_{\mathrm{U}_i} = N_{\mathrm{L}_i} = N/2$. Note that we ignore the centre particle in these calculations, otherwise there is an error on M_i of the order N_i^{-2}. Clearly, M_i is a function of r_{mix} (since the number of particles will be a function of r_{mix}) and so it is necessary to choose r_{mix} larger than the average interparticle spacing but smaller than the bulk features of the system such as fluid spacing or obstacle sizes. If r_{mix} is too small then we will have poor statistics but if it is too large it will no longer be local.

The utility of the expression presented above can be illustrated with a few test cases. Consider a particle i surrounded by particles of the same type. We would consider this particle to be completely unmixed and thus the expression gives us $M_i = 0$. Next,

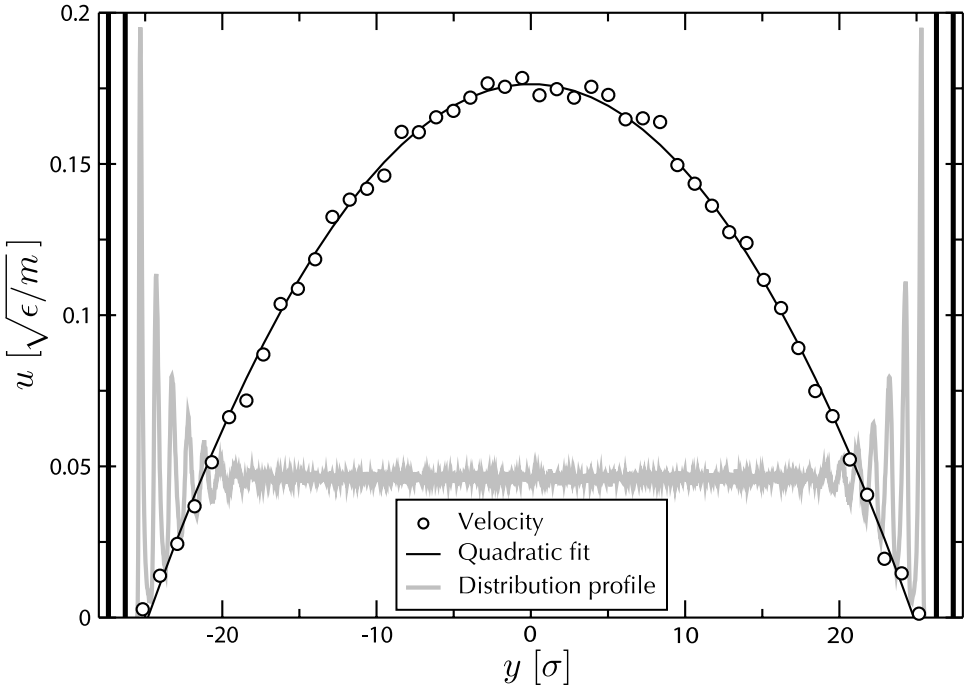

Figure 3. Velocity data taken as averages along 50 slices in the x direction (circular data points) and a fit to the data using Equation 2 (solid black curve) with y_0 and η as free parameters yielding $y_0 = 24.83 \pm 0.20\ \sigma$ and $\eta = 12.20 \pm 0.10\ \sqrt{m\epsilon}/\sigma$. The force on each particle is $mg = 0.005\ m\sigma/\tau^2$. Also shown, with arbitrary units, is the particle distribution profile demonstrating the positions of the fixed wall particles (black vertical lines) and the fluid layering near the walls (grey oscillating curve which levels off in the centre, demonstrating bulk properties there). We can see that the first layer of liquid is essentially immobile.

consider a case less obvious than the first, that the same particle is surrounded by particles all of a different type. The fluid is definitely not mixed as both species are not present in equal amounts. Therefore, our mixing function also gives a value of $M_i = 0$. Finally, consider half the particles surrounding particle i to be of like type and the other half to be of unlike type. Conceptually, this particle would be considered to be fully mixed and appropriately we obtain a mixing value of $M_i = 1$. The function $M_i(r_{\text{mix}})$ will blur the mixing level at an interface over a distance r_{mix}; for example, particles within a distance r_{mix} of the interface between two segregated fluids will have $M > 0$ when they are clearly not mixed but this is a minor point.

4. Results I: Hydrodynamic Properties

In order to generate a Poiseuille flow we have applied a constant force on each fluid particle in the system. In a similar fashion to a pressure difference, and due to friction at the walls, this method has been shown to reproduce the desired Poiseuille flow characteristics in MD simulations [27]. For a basic channel with straight, molecularly smooth walls, no obstacles (so $L = 559.02\ \sigma$), an external acceleration of $g = 0.005\ \sigma/\tau^2$

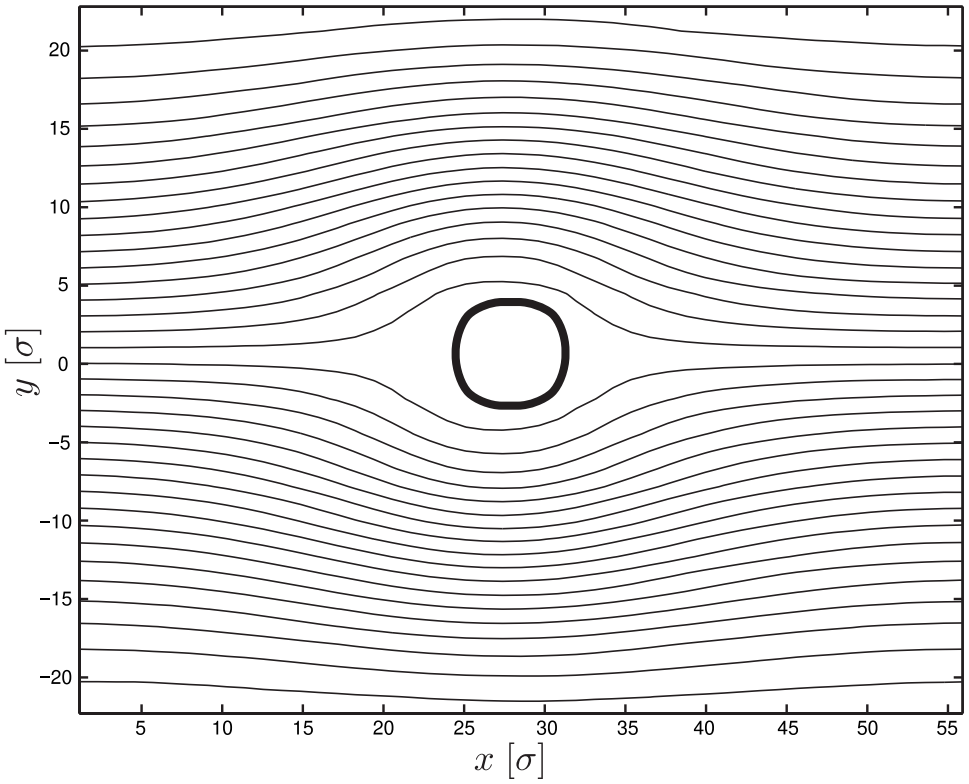

Figure 4. Streamlines demonstrating laminar flow around post of radius $R = 3.77\ \sigma$. Flow is generated by applying a force of $mg = 0.025\ m\sigma/\tau^2$ to fluid particles in a $W = 55.9\ \sigma$ by $L = 55.9\ \sigma$ two-dimensional channel. Streamlines were found by taking contours of the streamfunction ψ which itself was found by integrating the velocity field according to the definitions $\partial\psi/\partial y = u$ and $\partial\psi/\partial x = -v$ where u and v are the x and y components, respectively, of the fluid velocity. The simulation was run for 4×10^7 steps ($t = 4 \times 10^5\ \tau$) in order to obtain smooth data.

or force mg applied to each fluid particle, and periodic boundary conditions along x we recover a nearly quadratic flow profile (see Fig. 3). Using Equation 2 we can perform a fit to the flow profile data and recover the effective position of the wall (the true position is indeterminate due to the soft nature of our MD beads) $y_0 = 24.83 \pm 0.20\ \sigma$ and the shear viscosity $\eta = 12.20 \pm 0.10\ \sqrt{m\epsilon}/\sigma$. We have defined the position of the wall as the position of no fluid slip (i.e., $u(y_0) = 0$). Furthermore, with the viscosity we can determine the Reynolds number from Equation 1. Using $h = 2y_0$ and $\bar{u} \simeq 0.1\ \sigma/\tau$ (which is appropriate for what we observe, see Fig. 3) we can calculate the Reynolds number for our flow to be approximately $\mathrm{Re} \simeq 2.84$, which is clearly in the laminar flow regime. This demonstrates that our MD fluid flow simulations are certainly in the laminar regime, and as such they are relevant for microfluidics.

As a further demonstration of laminar flow, we have performed simulations of fluid flow around a single obstacle. These simulations were on a system of dimensions $W = 55.9\ \sigma$ by $L = 55.9\ \sigma$ and with an applied force of $mg = 0.025\ m\sigma/\tau^2$ (which is larger than that used above to calculate Re and so this system will have a slightly larger

Reynolds number). A circular post of radius $R = 3.77\,\sigma$ (consisting of 32 LJ beads fixed in position) is placed in the centre of the channel and the fluid is forced to flow past the post. According to laminar flow, we should see smooth streamlines around the post as well as identical streamlines at the input and output, indicating that the presence of the post has not disrupted the flow before and after the post (this has been observed previously in 2D MD simulations [28]). We observe exactly this in Fig. 4 where the streamlines are presented (calculated from the time-averaged velocity field). It is due to this property that we believe posts will not enhance mixing in channels.

From a simulation of a system similar to the one above but lacking the solid post the diffusion coefficient D was calculated from the Einstein expression [23]. For diffusion in one dimension across the channel in the y-direction the diffusion coefficient is $D_y = (3.25 \pm 0.14) \times 10^{-2}\,\sigma\sqrt{\epsilon/m}$. From this value we can calculate the Peclet number from Equation 3 (again, using $\bar{u} \simeq 0.1\,\sigma/\tau$ and $y_0 = 24.83 \pm 0.20\,\sigma$) which yields $\mathrm{Pe} \simeq 75 \gg 1$. This clearly demonstrates that advection is dominant over diffusion in this system and mixing will be slow.

5. Results II: Purely Diffusive Mixing With No Obstacles

As a benchmark result, we ran simulations of two physically identical fluid types (A and B) in a channel with a Poiseuille flow profile (generated by a uniform force $mg = 0.005\,m\sigma/\tau^2$ in the x direction). The fluids are initially separated along the midplane of the channel (type A for $y > 0$ and type B for $y < 0$) and they are bounded by walls at $y = \pm y_0$. We have applied periodic boundary conditions in the x direction with the modification that particles flowing past the boundary on the right side have their type (A or B) reset so that the two fluids are always entering the channel in a completely unmixed state (again, type A for $y > 0$ and type B for $y < 0$). The channel length is $L = 559.02\,\sigma$ and we have $y_0 = 24.83 \pm 0.20\,\sigma$.

The flow is purely laminar and thus, as described in Section 2.1, the only drive for mixing is the diffusion of one fluid species into the other. We calculate the mixing associated with each particle using Equation 8 (with $r_{\mathrm{mix}} = 6\,\sigma$, a value we found to strike a balance between computational efficiency and good statistical averaging) and then take averages of r_{mix} in (i) small xy bins and (ii) slices along x. These data can be seen in Fig. 5. We can see that as the fluid travels further down the channel its mixing level rises (Fig. 5a) as the two fluid species diffuse into each other. Furthermore, we can visualize the mixing front in two dimensions in Fig. 5b which exhibits an initial $\sqrt{x}$ form and then displays an inflection point about midway along the channel, the same qualitative structure as the flow-diffusion profile for Poiseuille flow given by Equation 6. This is expected since the mixing front should roughly correspond to the average position of the diffusing particles in Poiseuille flow. Clearly, with our channel we do not achieve 100% mixing but we can use the Peclet number in order to obtain an estimate on the length of channel L_0 required in order to obtain full mixing, $L_0 = \mathrm{Pe} \cdot y_0/2 \simeq 925\,\sigma$, which is nearly twice the channel length we use. The question that we explore in the

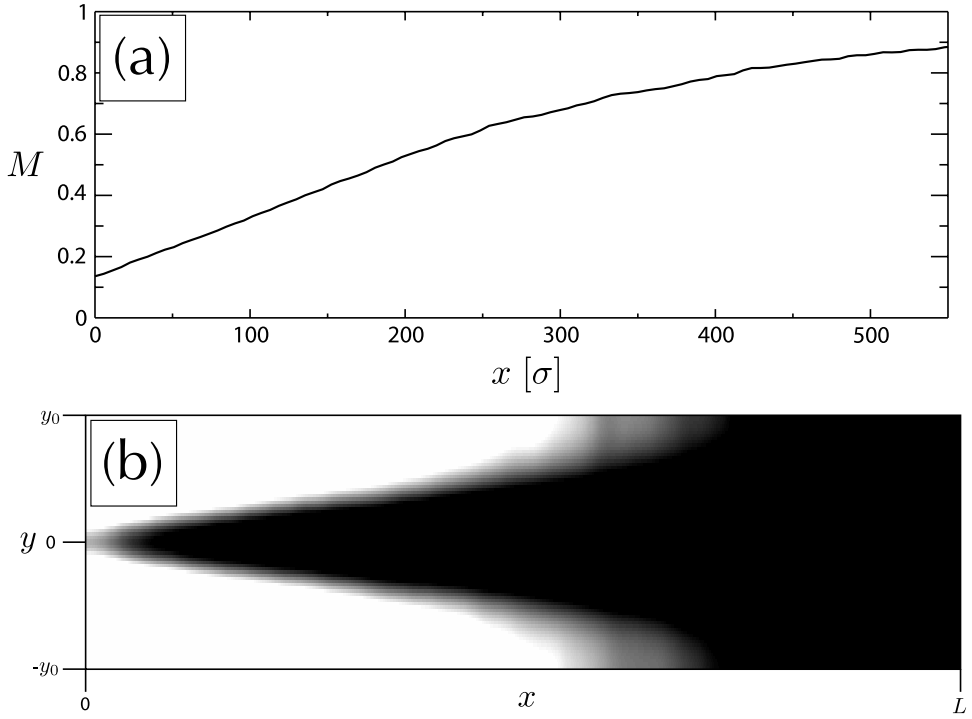

Figure 5. Mixing levels (using $r_{\text{mix}} = 6\,\sigma$) for a channel with no obstacles and smooth Poiseuille flow. (a) demonstrates average mixing level along the length of the channel in one hundred 5.59σ-wide slices. We observe the mixing level increase as the fluids flow along the channel and diffuse into each other. Note that $M \neq 0$ at $x = 0$ since there will be a finite level of mixing measured due to the contact between fluids at the initial interface (r_{mix} is finite). (b) demonstrates the mixing level averaged in 5.59σ-a-side square bins in xy and over time once the system has reached steady state. White represents $M < 0.5$ and black represents $M > 0.68$ with a grayscale continuum in between (therefore, white does not represent *unmixed* nor does black represent *mixed*). The values are chosen so that we can best observe the qualitative inflected shape of the mixing front which matches what is expected from the flow-diffusion profile for Poiseuille flow (see Fig. 2). The data contributing to this image has been modified by applying a Gaussian blur.

rest of this article is whether the addition of obstacles in this channel can increase the level of mixing.

6. Results III: Mixing With Obstacles

6.1. Prism-like Obstacle Configurations

Now, we take the previously mentioned system and place arrays of obstacles in the channel to explore their effect on the mixing efficiency of the channel. We have considered *prism*-like obstacle configurations (similar to those used by Wang *et al.* [12, 13]) as well as properly chosen deconstructions of these configurations in order to test the effect of prisms versus simplified obstacle placement. The exact configurations

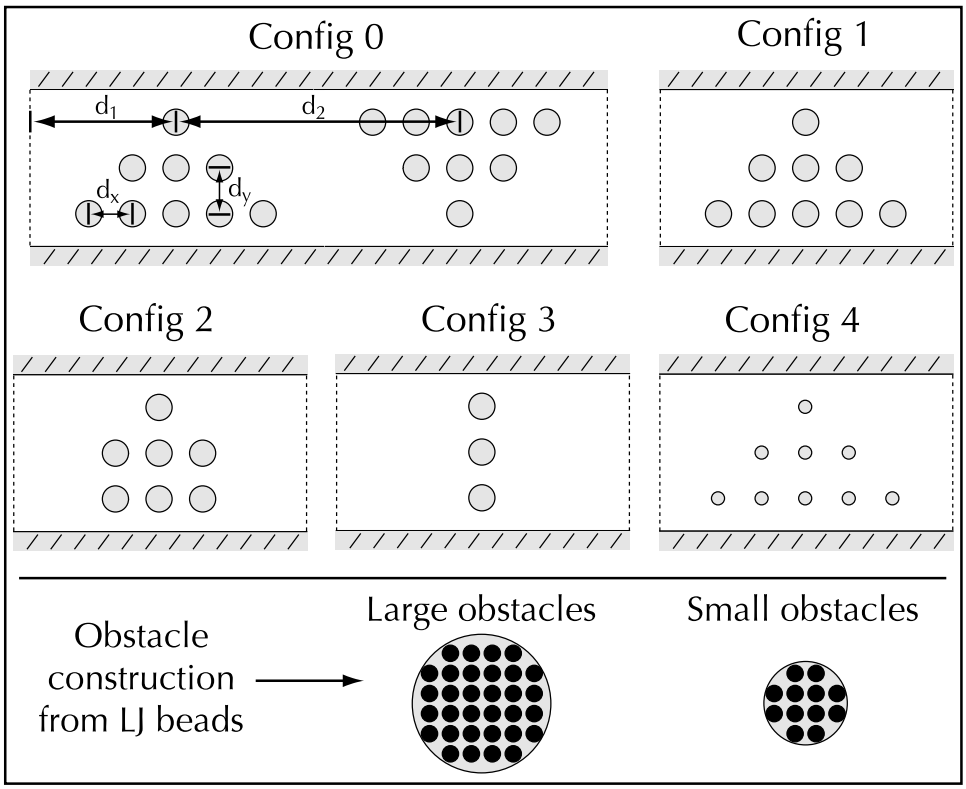

Figure 6. Schematics of the 5 obstacle configurations used in the MD simulations. Configuration 0 is used as the base and has two prism like structures inverted from each other. The centre of the first prism is a distance $d_1 = 67.08\,\sigma$ from the channel inlet and the centre of the second prism is a distance $d_2 = 100.62\,\sigma$ from the centre of the first. The obstacles are placed $d_{\rm x} = 16.77\,\sigma$ apart along x and $d_{\rm y} = 15.09\,\sigma$ apart along y and have a radius of $R = 3.77\,\sigma$. Each configuration following configuration 0 is formed by succesively removing some obstacles: First, the second prism. Then, obstacles from each end of the prism (so that configuration 3 is symmetric in the y direction). The final configuration is produced by reducing the radius of the circular obstacles in configuration 1 (radius is now $R = 2.26\,\sigma$). Also shown here is the exact Lennard-Jones bead configuration for each obstacle size.

used as well as their dimensions can be found in Fig. 6. Due to the reversibility of laminar flows the streamlines will be identical at the inlet and outlet of the channel whether or not obstacles are present (for a good discussion on this point, see the recent microfluidics book by Tabeling [29]). This concept was mentioned in the discussion of the Reynolds number in Section 2.1 and demonstrated for a single post in Section 4. The flow obstruction by the presence of obstacles has two effects: (i), a local disruption (i.e., flattening) of the flow profile that decays back into a parabolic profile eventually well past the obstacles, and (ii), increasing the length of the interfacial boundary per unit length along x by inducing a weak and localized lateral component to the flow.

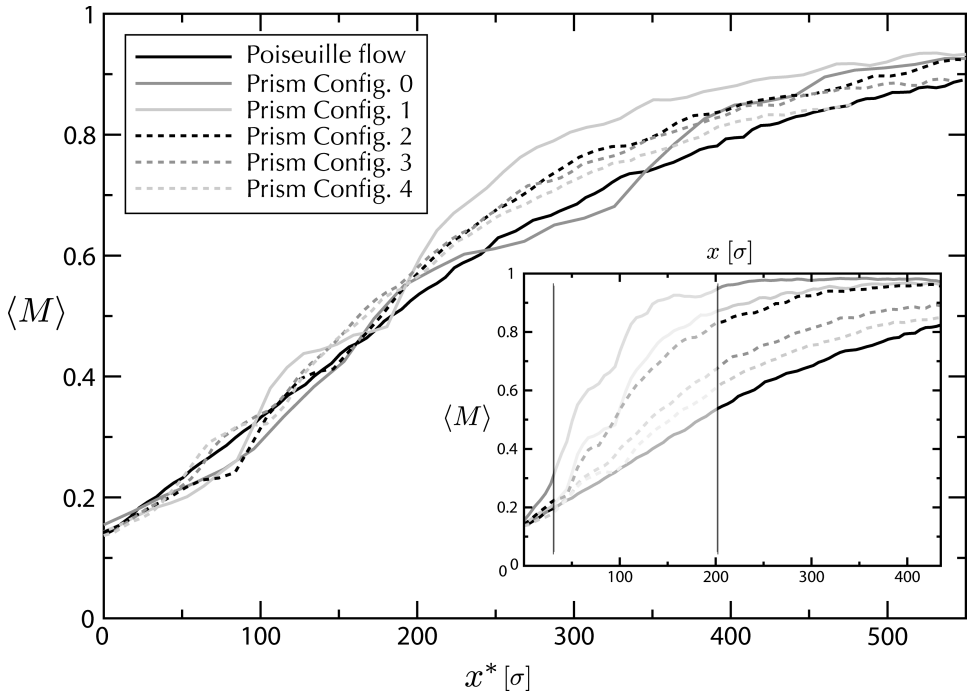

Figure 7. Mixing levels for all channels simulated ("Poiseuille flow" refers to the channel with no obstacles). The inset shows the raw data for each simulation averaged in 5.59σ-wide slices along x. The grey area shows the region affected by the presence of the obstacles (region defined as $x \in [33.54, 201.24]\,\sigma$, the maximum extent of the obstacles in configuration 0). The main figure compensates for different flow rates and the data for the obstacle-laden channels are scaled as if they have the same flow rate as the pure diffusion case. This is done for each case by the transformation: $x^* = x \cdot (\bar{u}_0/\bar{u})$ where $\bar{u}$ is the average flow rate for the simulation in question and $\bar{u}_0$ is the average flow rate for the Poiseuille case. The inset shows the data without this transformation.

6.2. Mixing Levels

We performed simulations on channels similar to those in Section 5 except with a shorter length ($L = 447.21\,\sigma$) and a stronger force ($mg = 0.01\,m\sigma/\tau^2$). As before, fluids enter the channel separated and diffuse as they flow down the channel except that now there is an additional contribution to the flow characteristics due to the presence of the obstacles. Average mixing values along the length of the channel were computed and are presented in Fig. 7 along with the data for the channel with no obstacles (pure diffusion). The inset shows the raw data which demonstrates larger mixing for channels with obstacles. However, each simulation does not have the same flow rate since we are keeping g constant, not $\bar{u}$, and different obstacle configurations and numbers will result in different flow rates. In general, a stronger acceleration is needed as the number of obstacles increases since they will pose as barriers to the fluid flow. In fact, some flow rates are over 50% smaller than the pure Poiseuille case due to the hydrodynamic resistance created by the obstacles.

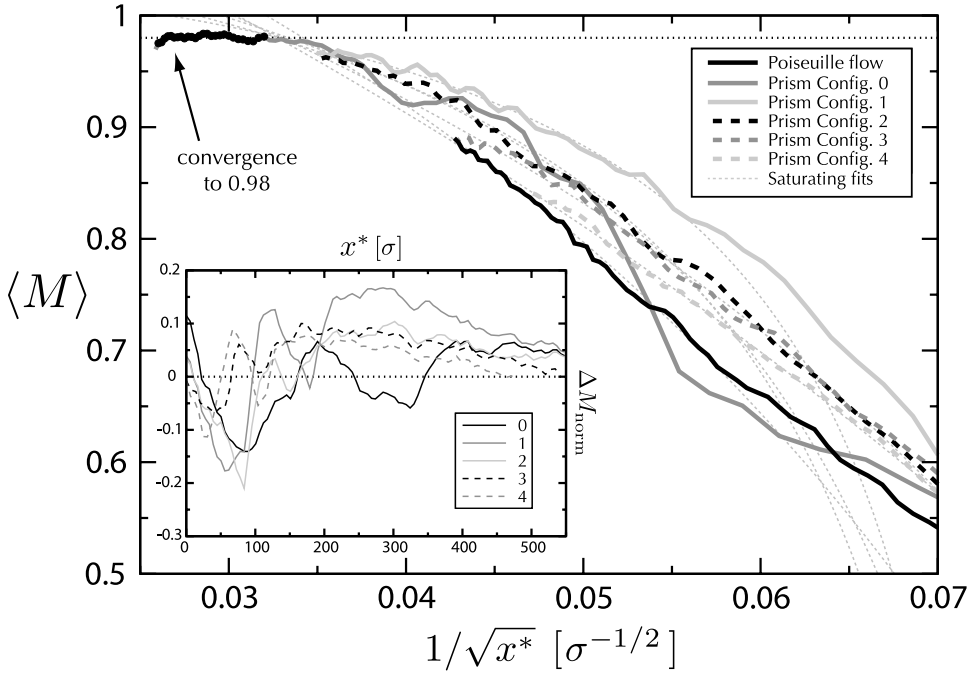

Figure 8. Inset: The difference between the mixing curves for the obstacle-laden channels and the purely Poiseuille flow channel. We can see a maximum of about 10%-20% difference in partial mixing about $x^* \in [200, 300]\ \sigma$ for obstacle configuration 1. For large x^* the difference decreases and they converge when $\langle M \rangle \simeq 1$ for all cases. Main plot: convergence to full mixing for large x^* using the transformation $1/\sqrt{x^*}$. We see the convergence to $\langle M \rangle \simeq 0.98$ for obstacle configuration 0 (the thin dashed line shows $\langle M \rangle = 0.98$)

From Equation A.4 (or Equation 6), the average length along the channel a particle travels while diffusing a certain distance (or equivalently, achieving a certain level of mixing) is proportional to the average velocity: $\langle l \rangle \propto \bar{u}$; therefore we scale the mixing data so that each obstacle-laden channel has the same flow rate as the channel with no obstacles (in absence of turbulence, such a rescaling can be done without changing the physics). This normalization operates as follows: $x^* = x \cdot (\bar{u}_0/\bar{u})$, where $\bar{u}$ is the average velocity in an obstacle laden channel and $\bar{u}_0$ is the average velocity in the Poiseuille case. We observe that the channels with obstacles have a higher level of mixing for about $x^* > 150\,\sigma$ which is after the obstacles will begin affecting the mixing (Fig. 7). However, since this difference decreases after about $x^* = 350\,\sigma$ (the curves converge) the enhanced level of mixing is merely due to the fact that we are measuring before the natural point of 100% mixing (i.e., $L_{\mathrm{M}} < L_0$).

This theory suggests that the distance required to achieve full mixing is unchanged in the presence of our obstacle configurations. All that is being accomplished is a transient deformation of the flow profile and under such conditions the mixing curves still converge for $\langle M \rangle \to 1$. Our channels are too short to observe total convergence (since $\mathrm{Pe} > L/2y_0$) but there is an onset of convergence for large x^* especially if we

look at the normalized difference between the mixing curves in the obstacle-laden cases ($\langle M(x^*)\rangle$) and the Poiseuille case ($\langle M_0(x^*)\rangle$):

$$\Delta M_{\text{norm}} = \frac{\Delta M}{\bar{M}} = \frac{\langle M\rangle - \langle M_0\rangle}{\frac{1}{2}\left(\langle M\rangle + \langle M_0\rangle\right)}. \tag{9}$$

This can be seen in the inset to Fig. 8 for each of the obstacle configurations.

The mixing curves should all converge at the same point and that should correspond to when they reach $\langle M\rangle = 1$. The mixing level seems to saturate around $\langle M\rangle = 0.98$ rather than 1.0 which we believe is due to the presence of the walls and the finite nature of r_{mix}. To examine this closer we transform the position by taking $\xi = 1/\sqrt{x^*}$. This will allow us to extrapolate for large x^* (the square root is used to filter the first order behaviour of diffusion which is of that form, see Section 2.2 for details). Convergence can clearly be seen in Fig. 8 for configuration 0. If we take $\langle M\rangle = 0.98$ as the measure of full mixing, then configurations 0 reaches the maximum at $x^* \simeq 937.5\,\sigma$. For the other configurations we will extrapolate using an empirical fit to a saturating function constrained to the last ∼15% of the transformed data. The fit follows the equation:

$$\langle M\rangle = \frac{M_1(\xi_0 - \xi)}{\xi_1 + (\xi_0 - \xi)} + M_0, \tag{10}$$

where M_0, M_1, ξ_0 and ξ_1 are the fitting parameters. The fits predict full mixing at $x^* \simeq 920.0\,\sigma$, $x^* \simeq 898.6\,\sigma$, $x^* \simeq 917.2\,\sigma$, $x^* \simeq 932.4\,\sigma$ and $x^* \simeq 856.0\,\sigma$ (for configurations 1, 2, 3, 4 and the purely diffusive case respectively). The cases with obstacles clearly increase the distance required for full mixing when compared to the purely diffusive case. The fits can be seen as light dashed curves in Fig. 8. All of these values lie near the position $x^* = 896.8\,\sigma \pm 4.5\%$ and thus all reach full mixing around the same point.

6.3. Lengthening of Mixing Interface due to Cross-Channel Flow

An aspect of the system that may affect the mixing characteristics is the effective amount of contact between the two fluid species, the *contact length*: L_{C}. In a plain channel with no obstacles the interface between the fluids (effectively the streamline that passes through $(x, y) = (0, 0)$) is straight and thus the contact length is equal to the length of the channel: $L_{\text{C}} = L$. However, if the fluids are perturbed laterally, then this streamline will follow a sinuous path down the channel and L_{C} will be the contour length of this streamline which will have the property: $L_{\text{C}} > L$.

In the presence of an asymmetric (in y) configuration of obstacles we observe that the fluid velocity in the channel acquires a y component that is not present in absence of these obstacles (see Fig. 9a). Furthermore, by looking at the calculated mixing values in two dimensions we determine that the fluid follows a sinuous path down the channel (indicated by the white line in Fig. 9b). If we estimate where the interface is (by following the maximum in the mixing function) we can determine the contour length of the interface and thus L_{C}. For obstacle configuration 1 (which is representative of the others) we find $L_{\text{C}} = 451.43\,\sigma$ which is ∼1% longer than the channel length L. From

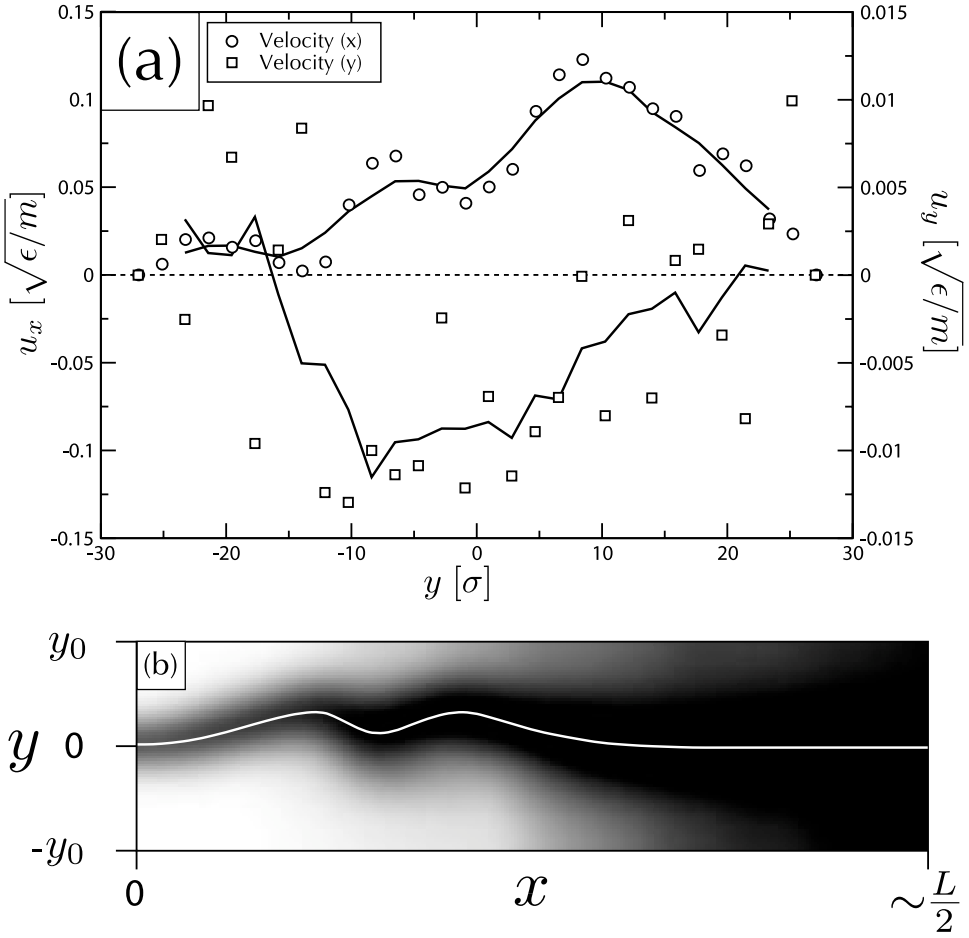

Figure 9. (a) The x and y components of the fluid velocity for obstacle configuration 1 (averaged over the regions in the vicinity of the prism and immediately after the prism, respectively). We clearly see that the obstacles resist the flow in regions (i.e., slices in y) containing more obstacles resulting in an asymmetric flow profile. Also, we see that after the prism the fluid velocity has acquired a nonzero y-component. (b) The mixing observed in two-dimensions shown for x between 0 and $L/2$ and with the same averaging bins as in Fig. 5. The white line shows the central streamline (determined by eye) which exhibits sinuous flow behaviour. The contour length of this line is ∼1% longer than the length of the system: $L_{\mathrm{C}} \simeq 1.01L$. The sinuous flow is damped out far from the obstacles and begins to return to a Poiseuille-like flow profile with no transverse component.

Equation 6, d and thus the position of the mixing front should scale (to first order) as $\sqrt{\langle l \rangle}$ and thus the difference in contact length we observe will result in the mixing front (approximately determined by d in Equation 6) being closer to the wall by less than one percent.

The calculation given above depends on the length L of the channel used in the experiment: a longer channel would result is a smaller difference between L and L_{C}. This can be partly alleviated by examining the flow only over the section of channel that is disturbed in the cross-channel direction by the presence of the obstacles (i.e., that

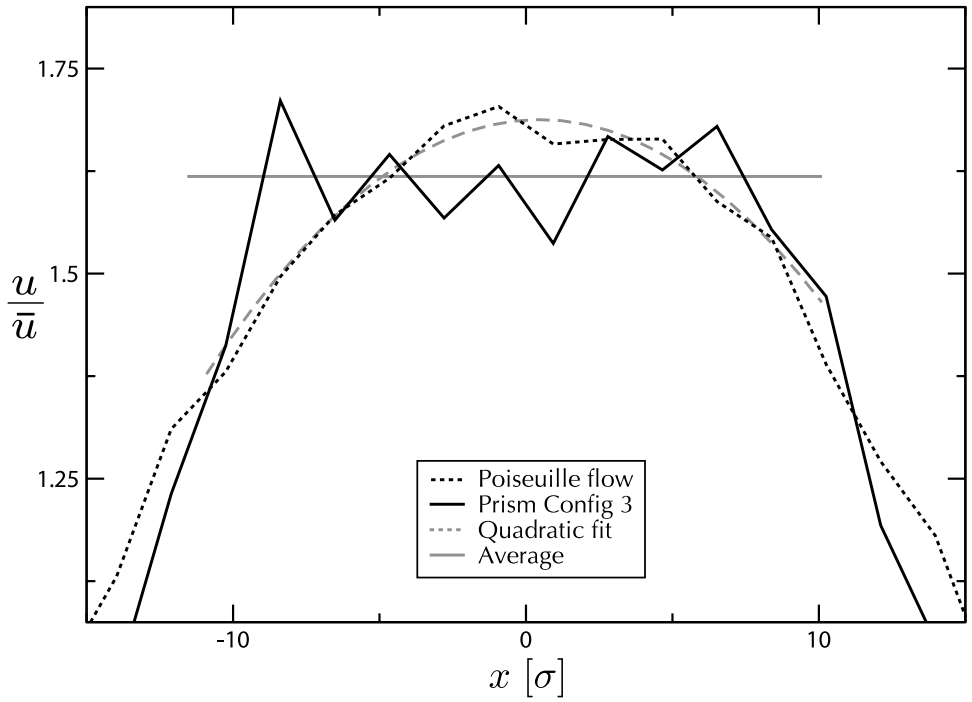

Figure 10. Flow profiles for the channel with no obstacles and for obstacle configuration 3. Each velocity profile has been normalized by its mean flow rate, $\bar{u}$. This representation allows us to see how the flow deforms in the presence of obstacles in comparison to the Poiseuille case. We can see that the obstacles deform the flow profile with repect to the quadratic Poiseuille case by flattening it. The solid grey line shows the average value of the flattened profile and the dashed grey line is a quadratic fit to the Poiseuille profile, both constrained to the region $x \in [-10, 10]\ \sigma$.

section of the channel over which the flow follows a sinuous path). This corresponds to $\sim L/2$ for obstacle configuration 1 (see Figure 9b) and so the mixing interface is only $\sim$2% longer over that section of the channel. Therefore, the lengthening of the mixing interface we observe will not significantly affect the mixing properties.

6.4. Flattened Flow Profile

We also measured the average flow profile over the range $67.08\,\sigma < x < 186.34\,\sigma$ immediately after the position of the obstacles configuration 3 (the symmetric obstacle configuration) in order to compare it with the flow profile from the Poiseuille case (see Fig. 10, where the flow has been normalized by $\bar{u}$ for comparison). It is clear by comparing the profiles that the presence of obstacles flattens the flow profile in the centre of the channel. This observation is less clear from the other obstacle configurations (not shown) as the asymmetric obstacle placement (in the y direction) produces an asymmetric flow profile. Furthermore, as we saw in the previous section, the flow profile also varies along the length of the channel and recovers a Poiseuille-like profile far from the obstacles. Essentially, the flow deformations are damped as the fluid travels farther

from the obstacles and we would expect to recover a Poiseuille flow far from the obstacles.

Since the flow profile is flattened in the centre of the channel, we expect this to affect the mixing. According to the theory outlined in Section 2.3, this effect should increase the level of partial mixing we observe. Clearly, the mixing levels we measured in Section 6.2 rise in the presence of obstacles, compared to the Poiseuille case, immediately after the position of the obstacles. Also, we observe that the configurations with asymmetric profiles (not shown) also appear to increase the level of mixing. Overall, these profiles are also "flatter" than the Poiseuille case. If the channel length is such that the outlet is immediately after the obstacles, then it would give the impression that the presence of obstacles increases mixing efficiency, when in fact only the partial mixing will have been improved. Unfortunately, both flattened and non-flattened flow profiles will reach full mixing at the same point.

7. Conclusions

We have presented a basic theory for diffusion (and thus mixing) in channels with both flat and Poiseuille flow profiles. Under conditions where the flow rate is the same then all channels of length greater than L_0 (which has a universal value for channels with the same flow rate) will achieve 100% mixing by the outlet. We have also proposed a function to quantify the level of mixing in a fluid and associate a unique value to each element in a system consisting of an ensemble of particles (such as a Molecular Dynamics simulation of Lennard-Jones beads). In macroscopic models (or experimental observations) this expression can be generalized in terms of densities or concentrations of the individual species.

We have predicted using theory and demonstrated with MD simulations that the presence of obstacles in channels with fluid flow will disrupt the flow by flattening the profile across the channel (at least over a finite channel length) and introduce a lateral component to the velocity. In systems where the flow is composed of two identically-interacting species, the former effect causes the measured mixing to be larger if the point of measurement is less than L_0 and the latter effect lengthens the contact between fluids but does not contribute much to mixing. It is the former effect, the flow profile flattening, that may lead to obstacles being considered as mixing enhancers in some channel configurations. Generally, one wishes to shorten the distance and/or time required to attain complete mixing and we have demonstrated that it cannot be accomplished by placing simple localised obstacle arrangements in microchannels.

In the future it would be interesting to explore modifications to the relative strengths of the attractive and repulsive components of the Lennard-Jones potential in order to simulate immiscible fluids. This technique can also simulate hydrophobicity and various degrees of wall wetting. It would also be of interest to examine the mixing properties of very small channels where the nanoscopic structure of the fluids becomes apparent and will affect the physical properties of the system. Furthermore, since we have used Molecular Dynamics to model this system it would be trivial to simulate

complex fluids, such as those composed of dimers, oligomers and polymers, a task that is difficult using traditional macroscopic models.

8. Acknowledgements

G. W. S. would like to acknowledge the financial support of a Natural Science and Engineering Research Council (NSERC) Discovery grant. E. C. J. O. would like to acknowledge the financial support of the Sun Microsystems of Canada Scholarship, the Nunatsiavut Government PSSSP and the University of Ottawa Admissions Scholarship. Furthermore, E. C. J. O. would like to thank F. Tessier, M. Kenward, S. Casault and M. Bertrand for discussions, assistance and support in the preparation of this work. E. C. J. O. would also like to thank C. Carrea for encouragement.

Appendix A. Probabilistic Derivation of the Poiseuille Flow-diffusion Profile

From the solution of the one-dimensional diffusion equation we have that the probability distribution for finding a particle in space and time is

$$p(y,t) = \sqrt{\frac{1}{4\pi Dt}} \exp\left(-\frac{y^2}{4Dt}\right). \tag{A.1}$$

For some parameter $\gamma(y,t)$ we can find its average value $\langle\gamma\rangle$ over all space and in the range $t \in [0,T]$ from the following [30]:

$$\langle\gamma\rangle = \frac{\int_{-\infty}^{\infty}\int_0^T p(y,t)\gamma(y,t)dtdy}{\int_{-\infty}^{\infty}\int_0^T p(y,t)dtdy}. \tag{A.2}$$

Let us define the distance along the channel a particle has travelled while diffusing a distance d across the channel as l (ignoring reflections from the channel walls). The average distance can be expressed as $\langle l\rangle = \langle u\rangle t_{\mathrm{D}}$ where $\langle u\rangle$ is the average velocity and $t_{\mathrm{D}} = d^2/2D$ is Einstein's relation for the average time taken for a particle to diffuse a distance d. We are assuming a Poiseuille flow profile that varies only in space given by

$$u(y) = u_0\left(1 - \frac{y^2}{y_0^2}\right).$$

Using the probabilistic arguments outlined above (with the temporal range $t \in [0, t_{\mathrm{D}}]$) we can calculate the average velocity to be

$$\langle u\rangle = u_0 - \frac{u_0 D}{y_0^2} t_{\mathrm{D}} = u_0\left(1 - \frac{1}{2}\frac{d^2}{y_0^2}\right). \tag{A.3}$$

This is as expected: the average speed at $d = 0$ should be the peak of the flow profile (u_0) since this is the centre of the channel and thus the maximum velocity and it reduces to $u_0/2$ at the wall ($d = y_0$) which is expected for Poiseuille flow. For particles starting in the centre ($y(t=0) = 0$) we calculate $\langle l\rangle$ by multiplying Equation A.3 by t_{D}:

$$\langle l\rangle = \langle u\rangle t_{\mathrm{D}} = \frac{u_0 d^2}{2D}\left(1 - \frac{1}{2}\frac{d^2}{y_0^2}\right), \tag{A.4}$$

which demonstrates the correction to Equation 5 due to the quadratic nature of Poiseuille flow.

Appendix B. Discretized Derivation of the Poiseuille Flow-diffusion Profile

Given a generic flow profile which varies as a function of y, $u = u(y)$, we derive a numerical as well as analytic method of finding the average position along the channel a particle has travelled, $\langle l \rangle$, while diffusing a distance d across the channel. We will discretize the profile $y > 0$ into N slices. We will define the following: Δh is the width of the slices and h_i is the distance to the i^{th} slice from the centre of the profile. The distance h_i can be expressed as $h_i = i\Delta h$ where $i = 0, 1, \ldots, N-1, N$ and $h_N = y_0$. The velocity profile is discretized as $u_i = u(h_i)$.

We have discretized the velocity profile along y and consider each slice to have a constant velocity of u_i. Starting from the centre ($y = h_0 = 0$) the average time taken to diffuse to the end of the i^{th} slice can be found from Equation 4:

$$\langle t_{D_i} \rangle = \frac{h_i^2}{2D}.$$

Therefore, the average time a particle spends in the ith slice, $\langle t_i \rangle$, is the time taken to diffuse to the end of that slice minus the time taken to diffuse to the beginning of that slice (or to the end of the previous slice): $\langle t_i \rangle = \langle t_{D_i} \rangle - \langle t_{D_{i-1}} \rangle$. Now, we can write the average distance travelled along the length of the channel (in the direction of the flow) while a particle is in the i^{th} slice, $\langle \lambda_i \rangle$, as this time multiplied by the velocity in the slice

$$\langle \lambda_i \rangle = u_i \langle t_i \rangle = u_i \left(\langle t_{D_i} \rangle - \langle t_{D_{i-1}} \rangle \right).$$

Therefore, the average distance travelled along the channel after diffusing to the n^{th} slice is

$$\begin{aligned} \langle l_n \rangle &= \sum_{i=1}^{n} \langle \lambda_i \rangle = \sum_{i=1}^{n} u_i \left(\langle t_{D_i} \rangle - \langle t_{D_{i-1}} \rangle \right) \\ &= \frac{1}{2D} \sum_{i=1}^{n} u_i \left(h_i^2 - h_{i-1}^2 \right). \end{aligned}$$

We can rewrite the inner portion as follows

$$h_i^2 - h_{i-1}^2 = (h_i + h_{i-1})(h_i - h_{i-1}) = \Delta h (h_i + h_{i-1})$$

and so the sum is now

$$\langle l_n \rangle = \frac{1}{2D} \sum_{i=1}^{n} u_i (h_i + h_{i-1}) \Delta h. \tag{B.1}$$

This equation represents a numerical method of solving $\langle l \rangle$ as a function of d (where $d = h_n$) by discretizing the spatial coordinate and the velocity profile.

If we take the limit of Equation B.1 as $\Delta h \to 0$:

$$\lim_{\Delta h \to 0} \langle l_n \rangle = \lim_{\Delta h \to 0} \frac{1}{2D} \sum_{i=1}^{n} u_i (h_i + h_{i-1}) \Delta h \tag{B.2}$$

then we can turn it into an integral over h:

$$\begin{aligned}\langle l\rangle &= \frac{1}{2D}\int_0^d u(h)(h+h)dh \\ &= \frac{1}{D}\int_0^d u(h)hdh. \end{aligned} \tag{B.3}$$

This expression can give an analytic result but may not be useful in all cases (such as if $u(y)$ cannot be integrated or is only known numerically). Note that this entire treatment is for a particle diffusing from the centre of the channel towards the wall at $y = y_0$. However, due to the symmetry of the velocity profile the result will hold for a particle diffusing from the centre in the negative y direction as well.

As an example, we substitute the Poiseuille profile for $u(h)$ (from Equation 2) and evaluate the integral in Equation B.3:

$$\begin{aligned}\langle l\rangle &= \frac{u_0}{D}\int_0^d \left(1-\frac{h^2}{y_0^2}\right)hdh \\ &= \frac{u_0 d^2}{2D}\left(1-\frac{1}{2}\frac{d^2}{y_0^2}\right), \end{aligned} \tag{B.4}$$

which demonstrates the correction due to the quadratic nature of the profile. We can see that the method derived here gives the same result as the probabilistic method derived in Appendix A.

References

[1] Sudarsan A P and Ugaz V M. Multivortex micromixing. *Proceedings of the National Academy of Sciences*, 103:7228, 2006.

[2] Lin C H, Fu L M, and Chien Y S. Microfluidic T-Form Mixer Utilizing Switching Electroosmotic Flow. *Anal. Chem.*, 76:5265–5272, 2004.

[3] El Moctar A O, Aubry N, and Batton J. Electro-hydrodynamic micro-fluidic mixer. *Lab Chip*, 3:273–280, 2003.

[4] Stroock A D and Whitesides G M. Controlling flows in microchannels with patterned surface charge and topography. *Acc. Chem. Res*, 36:597–604, 2003.

[5] Kuksenok O, Yeomans J M, and Balazs A C. Using patterned substrates to promote mixing in microchannels. *Phys. Rev. E*, 65:31502, 2002.

[6] Chen C-K and Cho C C. Electrokinetically-driven flow mixing in microchannels with wavy surfaces. *Journal of Colloid and Interface Science*, 312:470–480, 2007.

[7] Knight J B, Vishwanath A, Brody J P, and Austin R H. Hydrodynamic focussing on a silicon chip: mixing nanoliters in microseconds. *Phys. Rev. Lett.*, 80:17, 1998.

[8] Stroock A D et al. Chaotic Mixer for Microchannels. *Science*, 295:647–651, 2002.

[9] Nguyen N T and Wu Z. Micromixers–a review. *J. Micromech. Microeng.*, 15:R1–R16, 2005.

[10] Hessel V, Löwe H, and Schönfeld F. Micromixers–a review on passive and active mixing principles. *Chemical Engineering Science*, 60:2479–2501, 2005.

[11] C.Y. Lee, C.L. Chang, Y.N. Wang, and L.M. Fu. Microfluidic mixing: A review. *International Journal of Molecular Sciences*, 12(5):3263–3287, 2011.

[12] Wang H, Iovenitti P, Harvey E, Masood S, and Deam R. Mixing of liquids using obstacles in microchannels. *Proceedings of SPIE*, 4590:204, 2001.

[13] Wang H, Iovenitti P, Harvey E, and Masood S. Optimizing layout of obstacles for enhanced mixing in microchannels. *Smart Mate. and Struct.*, 11:662–667, 2002.

[14] Bhagat A A S, Peterson E T K, and Papautsky I. A passive planar micromixer with obstructions for mixing at low Reynolds numbers. *J. Micro. Mech.*, 17:1017–1024, 2007.

[15] Wang C T and Hu Y C. Mixing of liquids using obstacles in Y-type microchannels. *Tamkang Journal of Science and Engineering*, 13(4):385–394, 2010.

[16] Wang C T, Shaw C K, and Hu T Y. Optimization of flow in microbial fuel cells: An investigation into propoting micro-mixer efficiency with obstacle. *Tamkang Journal of Science and Engineering*, 14(1):25–31, 2011.

[17] Bhagat A A S and PapautskyI. Enhancing particle dispersion in a passive planar micromixer using rectangular obstacles. *J. Micro. Mech.*, 18:085005, 2008.

[18] Thompson P A and Troian S M. A general boundary condition for liquid flow at solid surfaces. *Nature*, 389:360–362, 1997.

[19] Koplik J and Banavar J R. No-slip condition for a mixture of two liquids. *Phys. Rev. Lett.*, 80:5125–5128, 1998.

[20] Priezjev N V, Darhuber A A, and Troian S M. Slip behavior in liquid films on surfaces of patterned wettability: Comparison between continuum and molecular dynamics simulations. *Phys. Rev. E*, 71:41608, 2005.

[21] Dufresne E R, Altman D, and Grier D G. Brownian dynamics of a sphere between parallel walls. *Europhys. Lett.*, 53:264–270, 2001.

[22] Anekal S G and Bevan M A. Self-diffusion in submonolayer colloidal fluids near a wall. *J. Chem. Phys*, 125:034906, 2006.

[23] Rapaport D C. *The Art of Molecular Dynamics Simulation*. Cambridge University Press, Cambridge, 1995.

[24] Soddeman T, Dünweg B, and Kremer K. Dissipative particle dynamics: A useful thermostat for equilibrium and nonequilibrium molecular dynamics simulations. *Phys. Rev. E*, 68:046702–1–8, 2003.

[25] Peters E A J F. Elimination of time step effects in dpd. *Europhys. Lett.*, 66:311–317, 2004.

[26] Camesasca M, Manas-Zloczower I, and Kaufman M. Entropic characterization of mixing in microchannels. *J. Micromech. Microeng.*, 15:2038–2044, 2005.

[27] Koplik J and Banavar J R. Continuum deductions from molecular hydrodynamics. *Annu. Rev. Fluid Mech.*, 27:257–292, 1995.

[28] Ishiwata T, Murakami T, Yukawa S, and Ito N. Particle Dynamics Simulations of the Navier-Stokes Flow with Hard Disks. *Int. J. Mod. Phys. C*, 15:1413–1424, 2004.

[29] Tabeling P. *Introduction to Microfluidics*. Oxford University Press, USA, Oxford, 2006.

[30] Strauss W A. *Partial Differential Equations: An Introduction*. John Wiley & Sons, Inc., New York, 1992.